Nucl. Fusion **51** (2011) 083018 (10pp) doi:10.1088/0029-5515/51/8/083018

Advances towards QH-mode viability for ELM-stable operation in ITER

A.M. Garofalo[1], W.M. Solomon[2], J.-K. Park[2], K.H. Burrell[1], J.C. DeBoo[1], M.J. Lanctot[3,a], G.R. McKee[4], H. Reimerdes[3,b], L. Schmitz[5], M.J. Schaffer[1] and P.B. Snyder[1]

[1] General Atomics, PO Box 85608, San Diego, CA 92186-5608, USA
[2] Princeton Plasma Physics Laboratory, PO Box 451, Princeton, NJ 08543-0451, USA
[3] Department of Applied Physics and Applied Mathematics, Columbia University, 2960 Broadway, New York, NY 10027-6900, USA
[4] Department of Engineering Physics, University of Wisconsin-Madison, Madison, Wisconsin, USA
[5] Physics and Astronomy Department, University of California-Los Angeles, PO Box 957099, Los Angeles, CA 90095-7099, USA

E-mail: garofalo@fusion.gat.com

Received 14 January 2011, accepted for publication 9 June 2011
Published 12 July 2011
Online at stacks.iop.org/NF/51/083018

Abstract
The application of static, non-axisymmetric, nonresonant magnetic fields (NRMFs) to high beta DIII-D plasmas has allowed sustained operation with a quiescent H-mode (QH-mode) edge and both toroidal rotation and neutral beam injected torque near zero. Previous studies have shown that QH-mode operation can be accessed only if sufficient radial shear in the plasma flow is produced near the plasma edge. In past experiments, this flow shear was produced using neutral beam injection (NBI) to provide toroidal torque. In recent experiments, this torque was nearly completely replaced by the torque from applied NRMFs. The application of the NRMFs does not degrade the global energy confinement of the plasma. Conversely, the experiments show that the energy confinement quality increases with lower plasma rotation. Furthermore, the NRMF torque increases plasma resilience to locked modes at low rotation. These results open a path towards QH-mode utilization as an edge-localized mode (ELM)-stable H-mode in the self-heated burning plasma scenario, where toroidal momentum input from NBI may be small or absent.

(Some figures in this article are in colour only in the electronic version)

1. Introduction

One of the critical issues on the tokamak path to nuclear fusion as a source of electricity is realizing a high confinement mode of plasma operation (H-mode) without the large, pulsed heat loads to the wall that usually result from instabilities driven by the high pressure gradient of the H-mode edge pedestal. These periodic heat and particle ejections from the plasma core are caused by magnetohydrodynamic (MHD) instabilities known as edge-localized modes (ELMs). While they might provide sufficient edge particle loss to prevent helium ash accumulation in a burning plasma core, they also severely limit the lifetime of the divertor, a key particle and impurity control component of a tokamak. The size of ELMs can be reduced by increasing their frequency, which could be accomplished by ELM triggering using pellet injection [1] or using magnetic 'kicks' [2]. Alternatively, ELMs can be completely eliminated, albeit under limited parameter ranges, using static non-axisymmetric fields that are resonant with the equilibrium magnetic field near the plasma edge [3]. These ELM control approaches still need to be demonstrated under burning plasma conditions (e.g. low input torque, low collisionality).

Another possibility would be operation in a regime that exhibits the high confinement of H-mode without ELMs. Such a regime, the quiescent H-mode (QH-mode), [4] is ELM-stable as a result of increased edge particle transport due to an edge harmonic oscillation (EHO) [5], a benign rotating edge MHD mode. The additional particle transport driven by the EHO allows the plasma edge to reach a transport equilibrium at edge pressures and current densities just below the ELM stability boundary [4, 6]. Theory indicates the EHO is a saturated kink-peeling mode driven unstable by edge rotational shear at edge parameters near but below the ELM stability boundary in the absence of rotation [6]. This theory is independent of the sign of the rotational shear, which is consistent with experimental

[a] Present affiliation: Lawrence Livermore National Laboratory, 7000 East Avenue, Livermore, CA 94550, USA.
[b] Present affiliation: Association Euratom-Confederation Suisse, Centre de Recherches en Physique des Plasmas, Ecole Polytechnique Federale de Lausanne, Lausanne, Switzerland.

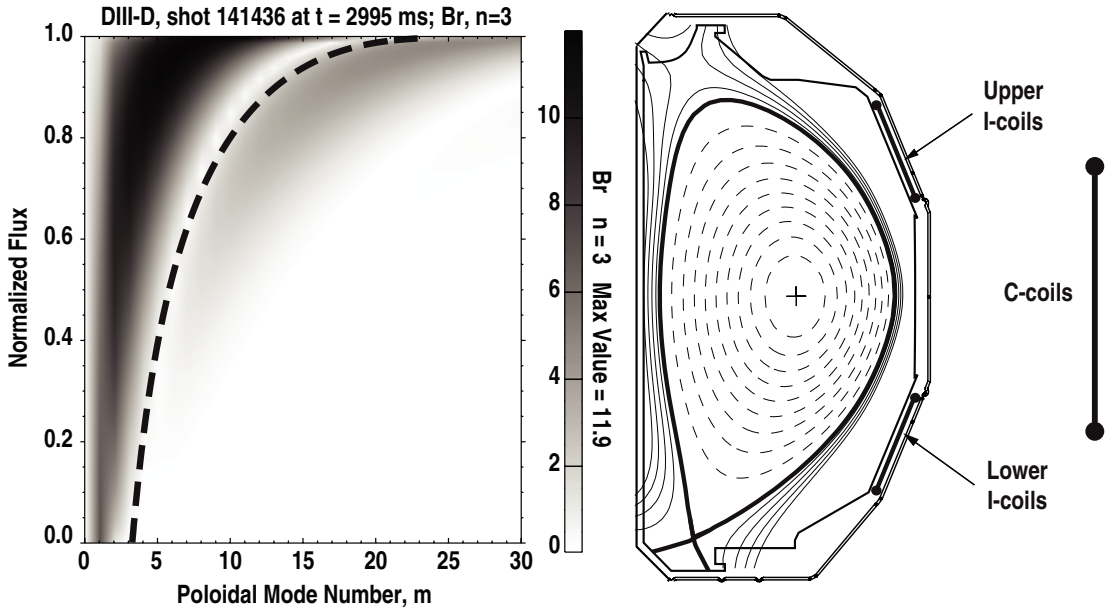

Figure 1. (*a*) Contour plot of the Fourier poloidal harmonic amplitudes of the $n = 3$ radial magnetic field perturbation applied by the I-coil ($I = 6.5$ kA), shown as a function of poloidal mode number m and minor radius. The loci of $m = nq$ resonance, indicated by the black dashed line, lie in a valley of field amplitude (i.e. the perturbation is almost purely nonresonant). (*b*) ITER-similar cross-section of the target plasma for the $n = 3$ field application, also indicating the I-coil and C-coil locations.

results [7] that QH-mode can be produced with edge rotation either in the direction of the plasma current or counter to it. In past experiments, this edge flow shear was produced using neutral beam injection (NBI) to provide toroidal torque. However, a self-heating fusion plasma will probably have near-zero NBI torque.

This paper reports on the first demonstration in a tokamak of the use of non-axisymmetric fields to achieve the ELM-stable regime of QH-mode, in the reactor-relevant regime of low-collisionality plasmas with significant normalized pressure and zero-net NBI torque [8]. Recent theoretical and experimental work has brought significant advances in the understanding of the interaction of static non-axisymmetric fields with a rotating high beta plasma. When a non-axisymmetric nonresonant magnetic field (NRMF) is applied to a near-stationary plasma, the toroidal rotation is accelerated towards a neoclassical 'offset' rotation rate, which is in the direction opposite to the plasma current (counter-I_p) [9, 10]. This magnetically driven torque provides a new knob to control the plasma rotation, and can be utilized to provide a counter-rotation profile that is suitable for QH-mode operation with no net NBI torque. In the experiments described in this paper, the NBI torque was completely replaced by the torque from applied NRMFs.

QH-mode without NBI torque could be an attractive regime for ITER [11]. Based on pedestal stability calculations, ITER is predicted to operate on the peeling stability boundary, where QH-mode can exist [12]. However, ITER is expected to operate with relatively small co-I_p NBI torque, which by itself may not yield the edge rotation shear necessary for QH-mode. The DIII-D NBI torque equivalent (with respect to the driven toroidal rotation) to the NBI torque expected in ITER is very small: about an order of magnitude smaller than the NBI torque applied in standard DIII-D operation (see the appendix). The experiments presented in this paper provide a potential solution to the problem of insufficient NBI torque for QH-mode in ITER. NRMF-assisted QH-modes were obtained in DIII-D discharges with zero-net NBI torque, ITER-similar cross-section shape, normalized pressure and confinement quality values at or above the ITER baseline targets, and pedestal collisionality at or below the ITER expected value. These results suggest that an ITER baseline scenario with QH-mode edge may be possible. Furthermore, comparisons of the observed NRMF torque to neoclassical theory predictions, also presented in this paper, show reasonable agreement, suggesting a remarkable degree of maturity in our understanding of NRMF torque physics. Further research, including experiments on different devices worldwide, would allow investigations on a wider range of plasma parameters and nonaxisymmetric field geometries, helping to improve our understanding of QH-mode physics and NRMF torque physics to the level required for confident extrapolations to ITER.

The rest of the paper is organized as follows: section 2 elucidates the torque balance in the DIII-D discharges with NRMF-assisted QH-mode, showing how the NRMF torque can replace the NBI torque in providing the edge rotation shear needed for QH-mode operation. Section 3 investigates the neoclassical physics associated with the NRMF, and compares predictions with experimental results. Sections 4 and 5 describe the effects of the NRMF respectively on confinement and on stability. Section 6 illustrates how these experiments have also allowed us to discriminate which type of rotation is important for maintaining the QH-mode edge. Section 7 summarizes the results and discusses future work.

2. NRMF-assisted QH-mode

Non-axisymmetric, mostly NRMFs of toroidal mode number $n = 3$ can be applied to DIII-D plasmas using the I-coil (see figure 1), a set of 12 picture-frame coils distributed toroidally

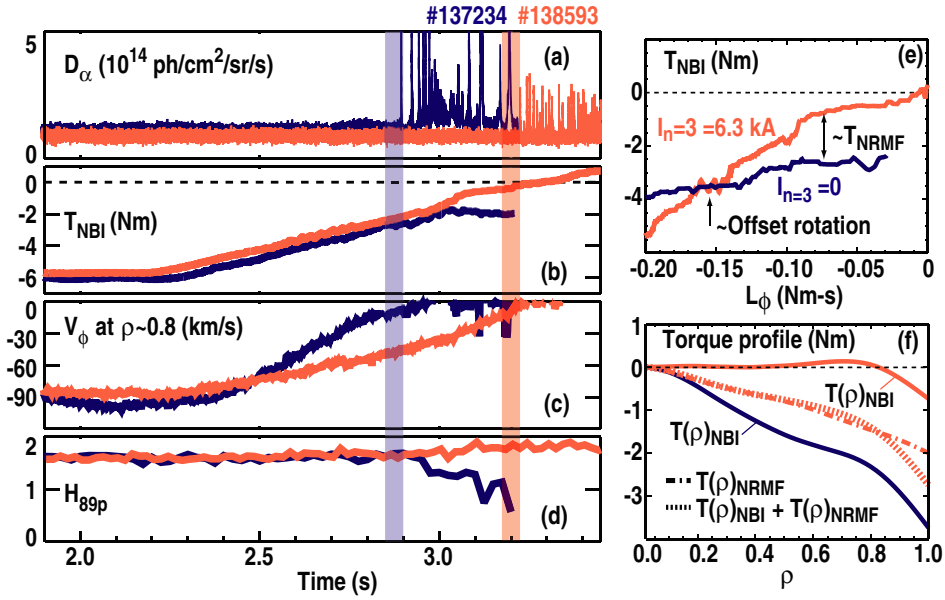

Figure 2. Comparison of NBI torque ramp-down discharges with constant NRMF applied (red traces, 6.3 kA of $n = 3$ I-coil current, discharge 138593) and with no NRMF (blue traces, discharge 137234). (*a*) Time histories of D_α light, showing QH-mode regime when bursting behaviour (from ELMs) is absent; (*b*) NBI torque; (*c*) plasma toroidal rotation at $\rho \sim 0.8$; (*d*) energy confinement quality; (*e*) discharge trajectories in the plane of NBI torque versus total toroidal angular momentum; (*f*) profiles of integrated torque density versus normalized minor radius calculated just before end of QH-mode phase (times indicated by vertical bands in (*a*)–(*d*)). Only four curves are shown in (*f*) since $T(\rho)_{\mathrm{NRMF}} = 0$ for discharge 137234.

and poloidally inside the vessel [13]. The experiments described in this paper used the largest perturbation deliverable by the I-coil, in which the largest single poloidal harmonic with $n = 3$ has a flux surface-averaged amplitude $\delta B \sim 12$ G at the plasma surface ($\delta B/B \sim 0.6 \times 10^{-3}$), ignoring any plasma response. To maximize the perturbation effect, the toroidal phase of the I-coil field is chosen so that the applied $n = 3$ field adds to a known, small $n = 3$ intrinsic error field (of magnitude equivalent, in terms of its effect on rotation, to the field from 0.7 kA of current in the I-coil configuration used). Target discharges are QH-mode plasmas with lower single null divertor cross-section shape, reactor-relevant pedestal collisionality, $\nu_e^* \sim 0.1$, monotonic safety-factor profile with $q \sim 1$ on axis and value at the 95% flux surface (q_{95}) of ~5.0, and β_N in the range 1.8 to 2.1 ($\beta_N = \beta/(I_p/aB)$ is the normalized β, where $\beta = \langle p \rangle/(B^2/2\mu_0)$ is the dimensionless plasma pressure, I_p the toroidal plasma current, a the plasma minor radius, and a the magnetic field strength). The plasma β_N is kept constant via feedback control of the NBI power. The feedback system can also control the injected NBI torque, T_{NBI}, by changing the mix of co- and counter-injected beams. T_{NBI} and plasma rotation are defined positive in the co-I_p direction. The plasma rotation is measured by charge exchange spectroscopy of the carbon impurity ion rotation.

The first evidence that static $n = 3$ NRMFs can maintain QH-mode with lower NBI torque than required without NRMFs is shown in figure 2. The QH-mode regime is ELM-stable as a result of increased edge particle transport due to a benign rotating edge MHD mode called the EHO [5]. Theory and experiments indicate that large edge rotational shear is a key requirement for existence of the EHO [6, 7]. Until recently, tokamak experiments relied on momentum injection from neutral beams to achieve the rotation shear required for access to QH-mode. For both plasma discharges in this figure, T_{NBI} is slowly ramped towards zero from ~−6 Nm at 2.2 s, at nearly constant injected power. In the discharge without the $n = 3$ NRMF (discharge 137234), the toroidal rotation drops quickly with the NBI torque, and reaches zero by $T_{NBI} \sim -2.5$ Nm, at which point first QH-mode is lost, then a locked mode spoils the confinement. The observation of zero rotation with finite NBI torque is consistent with an effective 'intrinsic' (self-generated) co-torque that balances the NBI torque at this point. In contrast, in the similar discharge with a constant $n = 3$ NRMF applied throughout the time range shown (discharge 138593), a larger counter-rotation is obtained for the same NBI torque, and the QH-mode is maintained until $T_{NBI} \sim 0$.

The magnitude of $T_{Intr} \sim 2.5$ Nm estimated in discharge 137234 is comparable to the observation in discharges where the intrinsic torque has been inferred directly (e.g. see figure 8 in [14]), and which have similar values of stored energy and plasma current, i.e. the plasma parameters believed important for the intrinsic rotation ('Rice scaling' [15]). The larger counter-rotation for the same NBI torque observed in the discharge with an applied $n = 3$ NRMF (138593) can be expected based on recent theoretical [9] and experimental [10] work showing that at slow counter-rotation, static NRMFs can accelerate a plasma. The torque driven by the NRMF tends to drag the plasma towards a neoclassical offset rotation velocity in the counter-I_p direction, $T_{NRMF} \propto -(V_\phi - V_\phi^0)$, with V_ϕ^0 the offset rotation. A simple comparison in figure 2(*e*) of the T_{NBI} required to obtain the same angular momentum in similar discharges with and without NRMF reveals the approximate magnitude of the NRMF torque, assuming the same intrinsic torque and angular momentum confinement time, τ_ϕ, in both discharges and neglecting dL_ϕ/dt in the torque balance equation (L_ϕ is the total toroidal angular

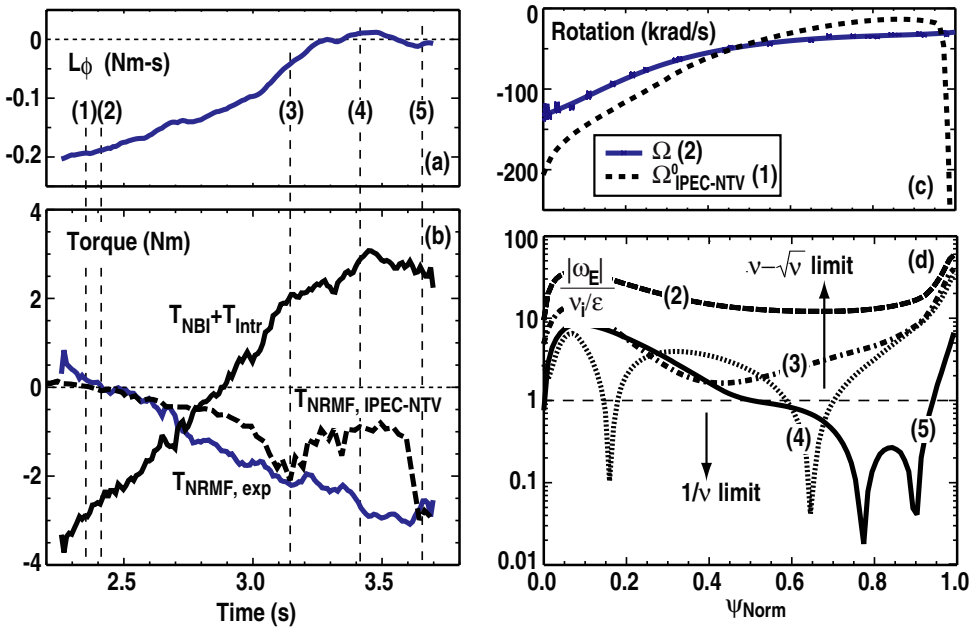

Figure 3. Time traces of (*a*) volume integrated toroidal angular momentum and (*b*) experimental torques (NBI, intrinsic, and NRMF) and theoretical NRMF torque in discharge 138593 of figure 2 during the NBI torque ramp-down. Radial profiles of (*c*) experimental and theoretically predicted offset rotation; (*d*) $|\omega_E|/\nu_i/\varepsilon$ evaluated at representative times during the angular momentum evolution. Labels (1), (2), (3), (4), (5) in (*c*) and (*d*) correspond to the times indicated by vertical dashed lines in (*a*) and (*b*).

momentum): $T_{\rm NBI} + T_{\rm NRMF} + T_{\rm Intr} - L_\phi/\tau_\phi = {\rm d}L_\phi/{\rm d}t$. The observation that the NRMF torque increases as the rotation approaches zero is consistent with the offset linear dependence of $T_{\rm NRMF}$ on the rotation. However, a nonlinear effect may also be playing an important role here. According to neoclassical theory calculations and a recent experimental verification [16], at this low rotation the NRMF torque is amplified by entering a regime where the radial electric field vanishes, leading to 'superbanana' particles with enhanced radial fluxes, which in turn exert a larger toroidal torque on the plasma. More details on this are given in section 3.

A more accurate transport analysis of the angular momentum balance in similar discharges with and without NRMF shows that the NRMF torque mostly compensates for the lower NBI torque in the discharge with the $n = 3$ NRMF applied. Described in [14], this transport analysis technique yields the profiles of the integrated NRMF and NBI torque densities shown in figure 2(f), confirming the simpler analysis. The figure compares integrated torque profiles at times just before the QH-mode phase ends in both discharges. Note that the rotation shear at the plasma edge depends on the integral of the torque density up to the edge (T), not on the local torque density distribution (η). This can be seen by writing the momentum balance equation,

$$mnR\frac{\partial V_\phi}{\partial t} = \eta + \frac{\partial}{\partial r}\left[mnR\left(\chi_\phi\frac{\partial V_\phi}{\partial r} - V_\phi V_{\rm pinch}\right)\right], \quad (1)$$

and integrating over the plasma volume, assuming steady state and neglecting the pinch contribution to the momentum flux relative to the diffusive term since the rotation is small at the edge while the gradient can be significant:

$$T\,({\rm edge}) = \int_{\rm axis}^{\rm edge}\eta\,{\rm d}V \approx -\left|mnR\left(\chi_\phi\frac{\partial V_\phi}{\partial r}\right)A\right|_{\rm edge}. \quad (2)$$

Here χ_ϕ is the angular momentum diffusivity and A is the area of the plasma cross-section.

Since a large edge rotation shear is a key condition for QH-mode, this analysis suggests that the $n = 3$ NRMF maintains QH-mode at lower NBI torque mostly by helping provide a sufficient total counter-torque on the plasma. However, the NRMF torque does not completely compensate for the lower NBI torque, therefore other effects must be at play. One such effect may be the density reduction observed when the $n = 3$ field is applied (discussed in section 3). Indeed, it is found that the NRMF torque normalized to the edge density almost exactly compensates for the lower (normalized) NBI torque. Using equation (2), this is sufficient to explain how the edge rotation shear is the same at the QH-mode threshold with or without NRMF. Edge rotation profiles for these two cases are presented in section 6, where the issue of understanding which species rotation is relevant for the QH-mode threshold will also be discussed.

3. NRMF torque physics

Results of theoretical modelling of the NRMF torque physics in discharge 138593 of figure 2 are shown in figure 3, in comparison with experimental data. Figure 3(a) shows the time evolution of the total toroidal angular momentum during the ramp-down of the NBI torque. The time trace of the volume integrated NBI plus intrinsic torque is shown in figure 3(b), together with a comparison of the volume integrated NRMF torque determined from transport analysis and the neoclassical theory prediction. The predicted and experimental NRMF torques are remarkably close, although some significant deviations exist. The theoretical prediction is obtained using, first, the IPEC code [17] to calculate the total magnetic perturbation, including the ideal MHD plasma response to

the external non-axisymmetric NRMF. Then, a generalized neoclassical model [18] is used to evaluate the resulting torque on the plasma, including the effects of precession rates and resonance with bouncing motion of trapped particles, and combining different collisionality regimes. Inputs to the code are the measured profiles of density, ion and electron temperature, carbon impurity ion toroidal rotation, and radial electric field measured at various times during the NBI torque ramp-down. Note that the code calculations have no free parameters, and that several approximations are made: one MHD equilibrium reconstruction, calculated for $t = 2.5$s (i.e. near the middle of the time range of interest), is used for all times. The measured carbon rotation is taken as the fluid rotation, ignoring any possible difference between the rotation speed of the various ions. In order to compare with the experiment, the predicted NRMF torque is scaled up by 23% to account for the (empirically determined) contribution of the intrinsic $n = 3$ error field (additive to the applied NRMF).

The resulting prediction of the NRMF torque evolution as the toroidal rotation is slowed down is in very good qualitative agreement with the experimental analysis. Quantitatively, the two results are close, with both significant deviations and points of excellent matching. In particular, a key feature such as the time at which the torque changes sign is in very good agreement between theory and experiment.

Figure 3(*c*) compares an experimental estimate of the offset rotation profile, which is obtained from the carbon rotation profile measured at the time when the experimental NRMF torque changes sign, with the theoretical offset rotation profile calculated at the time the predicted NRMF torque crosses zero. The profiles are fairly close throughout the minor radius, up to the last few per cent of the normalized flux. Quantitative neoclassical predictions may not be accurate near the H-mode pedestal, where the T_i gradient scale length becomes comparable to the banana width, thus standard neoclassical expressions may not be valid. Also, the rotation profile for which the total torque is zero may not necessarily match the true offset rotation profile, for which the torque density at all radii is expected to be zero.

The change in NRMF torque with changing angular momentum is probably not just due to the dependence $T_{\mathrm{NRMF}} \propto -(V_\phi - V_\phi^0)$. The proportionality in this equation and the offset rotation itself depend strongly on the neoclassical viscosity regime. Since a dominant NRMF effect believed responsible for the increased toroidal viscosity is the trapped-particle radial banana-drift, the boundaries between relevant neoclassical regimes depend on the value of the effective ion collisionality relative to the toroidal drift rate of the banana orbits (approximately equal to the toroidal component of the $E \times B$ drift, $\omega_E = E_r/RB_\theta$). As the total angular momentum decreases towards zero, ω_E also decreases, and the plasma moves from the $\nu - \sqrt{\nu}$ regime [19, 20] (where $\nu_{\mathrm{eff}} = \nu_i/\varepsilon < |\omega_E|$, with $\nu_{\mathrm{eff}} = \nu_i/\varepsilon$ the trapped–untrapped ion collision rate, and ε the plasma inverse aspect ratio) to the $1/\nu$ regime [19] (where $\nu_{\mathrm{eff}} = \nu_i/\varepsilon > |\omega_E|$). The plots in figure 3(*d*) of $|\omega_E|/\nu_i/\varepsilon$ evaluated at various times during the NBI torque ramp-down indicate that the peak at $t = 3.14$ s in the predicted NRMF torque corresponds to approaching a plasma transition from the $\nu - \sqrt{\nu}$ regime to the $1/\nu$ regime where the torque is reduced. However, as the NBI torque is further reduced and ω_E approaches zero, a singularity can occur as the precession frequency vanishes. Here, the step size of the banana orbits tends to become unbounded, and only collisions can limit the deviation from the flux surface, leading to plateau-like transport. This is a new regime, called the superbanana plateau regime [21]. The plots in figures 3(*a*)–(*d*) suggest that the predicted torque peak at angular momentum near zero at $t = 3.65$ s probably correspond to the plasma moving into the superbanana plateau regime. The experimental torque trace shows much smaller amplitude modulation, suggesting that the combination of different collisionality regimes in the model may not be fully realistic.

4. Effects on confinement

Application of the NRMF does not cause adverse impact on the global energy confinement. The global confinement quality, as measured by the confinement enhancement factor with respect to the ITER-89P L-mode confinement scaling [22], is unchanged during the QH-mode phase with or without the NRMF, as shown in figure 2(*d*). Figure 4 shows a comparison of the profiles of electron density and ion temperature before and during the NRMF application. After the NRMF turn-on, the density is reduced everywhere and the core ion temperature is increased. The electron temperature everywhere (not shown) and the pedestal ion temperature are nearly unchanged. Evidently, the reduction in the pedestal pressure is compensated by the improved core confinement. The density pump-out is an effect of non-axisymmetric field application observed also in other tokamaks [23], and whose physics explanation is under active investigation. Again, the confinement quality is unchanged during the QH-mode phase with or without the NRMF, other than a small dip immediately following the NRMF onset. This dip corresponds to a temporary return to ELMing behaviour, in some cases limited to the occurrence of one ELM.

It is consistently observed that the application of the $n = 3$ NRMF changes the character of the EHO. This is shown by the spectrum of measured magnetic fluctuations shown in figure 4. Before the NRMF application, the discharge is in QH-mode with an EHO having a typical spectrum with dominant toroidal mode number $n = 1$ and several harmonics. During the NRMF application, once the discharge goes back into QH-mode after a brief ELMing phase, the magnetic spectrum of the EHO has changed to one with dominant $n = 3$ and harmonics. The cause of this behaviour is under investigation. The EHO structure change may not be directly related to the mode number of the applied NRMF, since there are cases when the $n = 3$ NRMF changes the magnetic spectrum of the EHO to one with dominant $n = 2$ and harmonics. Furthermore, there are cases of QH-mode discharges where the EHO spectrum has dominant toroidal mode number $n = 3$ and harmonics even without NRMF applied. The EHO structure change following the $n = 3$ NRMF application may result from the effect of the NRMF on the equilibrium profiles and hence on the MHD stability of the edge modes.

The global energy confinement time of these NRMF-assisted QH-mode discharges is found to increase at lower net NBI torque magnitude. One example of this consistently observed behaviour is documented in figure 5. Here, a

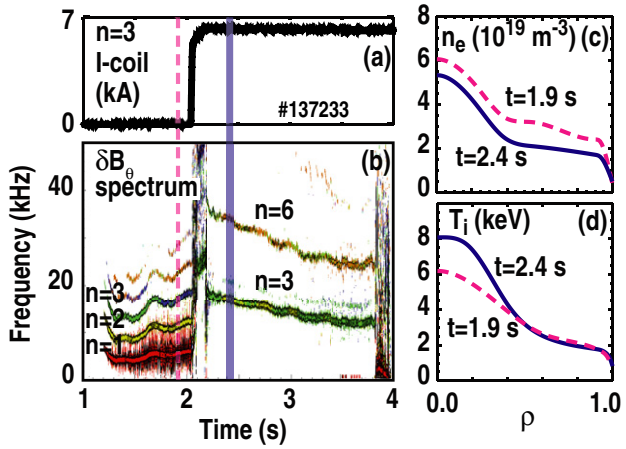

Figure 4. (*a*) I-coil current generating the $n = 3$ NRMF; (*b*) coloured contour plot of the toroidal mode number, n, spectrum of magnetic fluctuations versus frequency and time. Vertical lines indicate times before and after the NRMF application, for comparison of radial profiles of (*c*) electron density and (*d*) ion temperature.

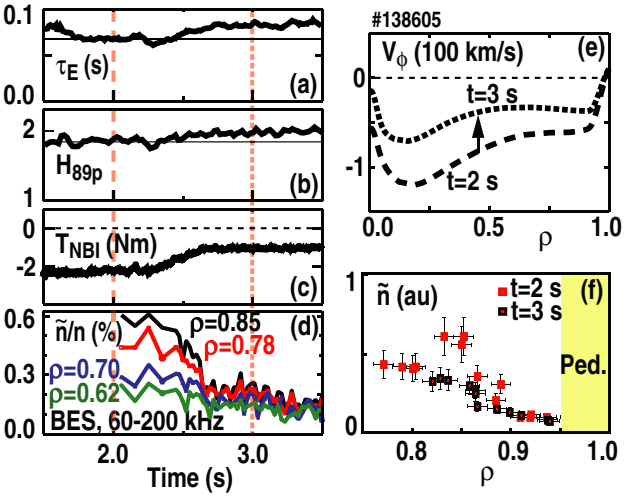

Figure 5. Confinement effects of NBI torque ramp-down. Discharge is terminated early by a fault of the plasma control system. Time histories of (*a*) thermal energy confinement time; (*b*) confinement quality; (*c*) NBI torque; (*d*) relative density fluctuation levels measured by BES at different normalized minor radii. Shaded vertical bands indicate time ranges relevant to the next panels: (*e*) radial profiles of toroidal plasma rotation; (*f*) radial profiles of relative density fluctuation level measured by DBS at high and low rotation.

discharge with $|T_{\rm NBI}|$ ramped down from 2 to 1 Nm shows that higher energy confinement time is achieved at lower $|T_{\rm NBI}|$. The improved confinement cannot be easily explained by a variation in MHD mode activity, which in fact is limited to the presence of an EHO with very low and constant amplitude (integrated over all frequencies) throughout the torque ramp-down. The improved confinement does correlate with reduced density fluctuation levels measured by the beam emission spectroscopy (BES) [24] and Doppler backscattering (DBS) [25] diagnostics, suggesting reduced turbulence. BES measurements (figure 5(*d*)) show the time evolution at several minor radii of electron density fluctuations

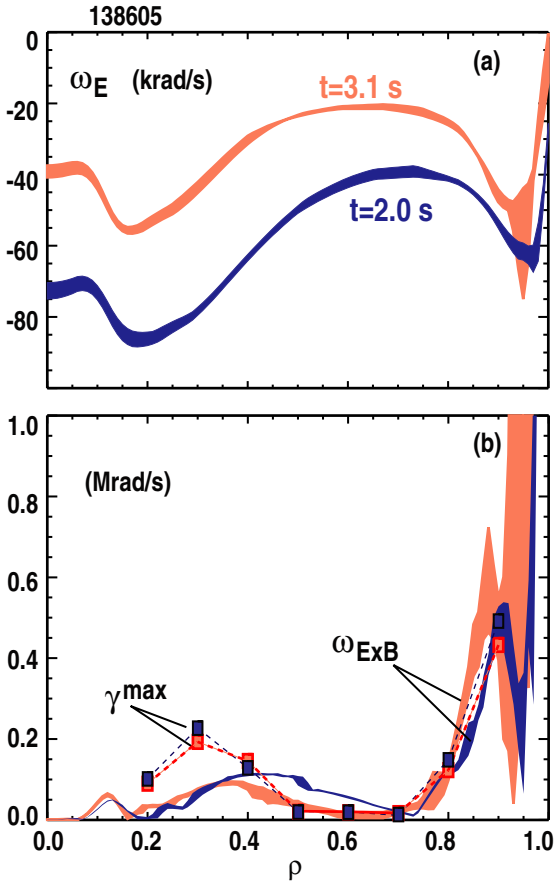

Figure 6. Comparison of radial profiles evaluated at high (blue) and low (red) rotation of (*a*) toroidal $E \times B$ rotation (ω_E); (*b*) absolute magnitude of the $E \times B$ shearing rate ($\omega_{E\times B}$) and calculated maximum growth rate for turbulence modes in the BES wavelength range ($\gamma^{\rm max}$). The vertical width of the curves indicates the uncertainty.

with poloidal wavenumber $k_\theta \sim 1.5\,{\rm cm}^{-1}$. In the plasma core, this wavenumber range is most often associated with ion temperature gradient modes, but may also correspond to trapped electron modes near the plasma edge. DBS measurements show fluctuations with poloidal wavenumber $k_\theta \sim 3.9\,{\rm cm}^{-1}$ in the electron density inboard of the H-mode pedestal ($k_\theta \rho_{\rm s} \sim 1$ with $\rho_{\rm s} = c_{\rm s} m_{\rm i}/eB_{\rm T}$, $c_{\rm s} = (kT_{\rm e}/m_{\rm i})^{1/2}$). This wavenumber is usually associated with trapped electron mode instabilities. DBS density fluctuations before and after $|T_{\rm NBI}|$ ramp-down are compared in figures 5(*f*). Both BES and DBS measurements show that density fluctuation levels decrease substantially at lower $|T_{\rm NBI}|$. The counter-rotation also decreases substantially at lower $|T_{\rm NBI}|$, and across the entire minor radius, as shown in figure 5(*e*).

The above observations may seem to suggest that the improved confinement with lower counter-rotation is not related to sheared flow stabilization of turbulence [26, 27]. However, further analysis indicates that the opposite is more likely true. The general criterion for flow shear suppression of fluctuations is that turbulence is affected when the shearing rate,

$$\omega_{E\times B} = \frac{(RB_\theta)^2}{B}\frac{\partial \omega_E}{\partial \psi},$$

becomes comparable to the linear growth rate of the turbulence [28]. As shown in figure 6, although ω_E decreases in magnitude after the $|T_{\rm NBI}|$ ramp-down (later analysis time, red curves), the magnitude of the shearing rate increases at surfaces with $\rho > 0.7$, i.e. where the BES measurements show strongest reduction in fluctuation levels. At these same radial locations, linear stability calculations with the TGLF code [29] show that the maximum growth rate for turbulence modes in the BES wavelength range is comparable to the shearing rate, possibly lower than the shearing rate calculated at lower counter-rotation. Therefore, the improved confinement is consistent with the paradigm of $E \times B$ flow shear suppression of turbulence. More cases are being analysed to see if a causal relationship can be established. More analysis is also needed to understand whether the $n = 3$ NRMF is playing a direct role in shearing rate modification or whether it simply facilitates access to low counter-rotation by its effects on stability, discussed in the next section of this paper. One hypothesis under consideration is that lower rotation may have higher $E \times B$ shear because of how the $V \times B$ and ∇P components of the radial electric field contribute to the shear when the rotation is in the counter-direction [30].

5. NRMF effects on stability

The DIII-D discharge shown in figure 7 demonstrates that QH-mode can be maintained down to zero-net NBI counter-torque when the $n = 3$ NRMF torque from the I-coil is augmented with an $n = 3$ field applied by the C-coil. The C-coil, a non-axisymmetric coil set external to the vessel and mainly utilized for $n = 1$ error field correction in these experiments, was used to increase the vacuum $n = 3$ field by ~50% at the plasma boundary in this discharge. However, the application of $n = 3$ NRMFs does more than just expand the QH-mode operating space to a zero-net NBI torque regime. The discharge of figure 7 shows high beta and high confinement operation of a plasma with very low density (line averaged density $<2.5 \times 10^{19}\,{\rm m}^{-3}$), and very low rotation (~0 at the $q = 2$ surface), i.e. conditions that typically lead to catastrophic locked modes.

The improvement of stability against locked modes in plasmas with zero-net or small counter-rotation is due to two separate NRMF physics mechanisms. Generally, a locked mode occurs when plasma rotation at a rational surface is no longer sufficient to shield a resonant error field. Without rotational shielding, the error field can easily open a magnetic island and, at finite beta, destabilize a metastable neoclassical tearing mode (NTM). Figure 2 showed that, by driving a counter-torque, the application of NRMFs maintains counter-rotation and avoids ELMs and locked modes as the NBI torque is reduced. A second mechanism is at work in the case shown in figure 8. Here, two similar discharges are compared, both with applied $n = 3$ NRMF from the I-coil and ramp-down of the NBI torque magnitude. Removing the $n = 3$ field at low torque in one discharge (138608) leads promptly to an $n = 1$ locked mode instability, while in the discharge with continued NRMF application (138611), stability is maintained even with lower NBI torque. One possible explanation is that a small magnetic island is already formed when the rotation comes down near zero while the $n = 3$ field is applied, and that the island may not grow as long as the $n = 3$ field is applied because of a mechanism that was originally proposed in [31]. In this hypothesis, the locally nonresonant $n = 3$ helical field enhances the perpendicular transport across the island, therefore weakening the helically perturbed bootstrap destabilization of the NTM. When the helical field is removed, the NTM suppression mechanism is removed as well, and the island starts to grow. This hypothesis is supported by the clear observation of locked rotation without mode growth in the stable discharge (138611). The rotation near the $q = 2$ surface in this discharge can be seen to lock to zero at $t = 3.6$ s, and remains firmly locked implying the presence of a small, stationary magnetic island. The island must be small since there is no sign of confinement degradation and a perturbation in the magnetic sensors is only barely observable. With the large $n = 3$ NRMF applied, the $m/n = 2/1$ island remains stable for several energy confinement times, and is destabilized only when the $n = 1$ error field correction is ramped down near the end of the discharge.

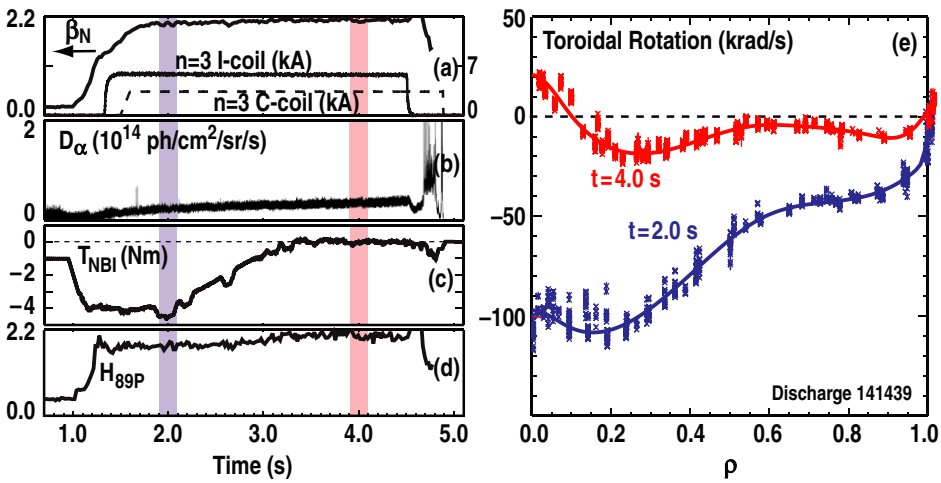

Figure 7. Demonstration of sustained QH-mode with zero-net NBI torque. Time histories of (*a*) $\beta_{\rm N}$, I-coil and C-coil currents; (*b*) D_α light; (*c*) NBI torque; (*d*) confinement quality. Shaded vertical bands indicate time ranges for toroidal rotation profiles shown in (*e*), before (blue, $t = 2.0$ s) and after (red, $t = 4.0$ s) the net NBI torque is removed.

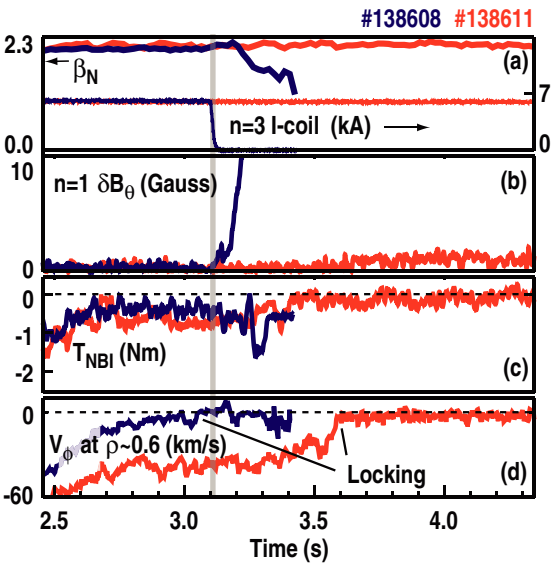

Figure 8. Comparison of discharges with and without removal of the $n = 3$ NRMF during phase of low NBI torque. Time histories of (*a*) β_N and I-coil current; (*b*) $n = 1$ locked mode detector signal; (*c*) NBI torque; and (*d*) toroidal plasma rotation at the approximate location of the $q = 2$ surface.

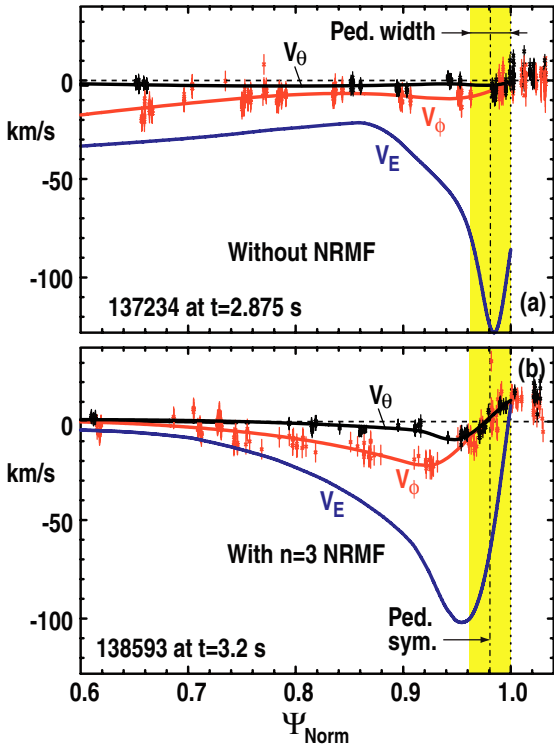

Figure 9. Comparison of the edge radial profiles of the toroidal rotation (V_ϕ), poloidal rotation (V_θ), and toroidal $E \times B$ rotation (V_E) measured at the QH-mode threshold observed in the discharges of figure 2. (*a*) Discharge 137234 without NRMF and (*b*) discharge 138593 with $n = 3$ NRMF applied. V_ϕ and V_θ are measured directly from the carbon impurity rotation, while V_E is determined from V_ϕ, V_θ, and the measured pressure profile.

The hypothesis of NTM inhibition by an externally applied helical field had been tested successfully in previous DIII-D experiments [32]. However, in those experiments the initial plasma rotation was large and co-directed. The application of an $n = 3$ field in that case led to rotation slowing down towards zero and reduction in confinement. In the new experiments reported here, the negative effects of the applied helical field are eliminated or reversed. In the counter-rotating plasma regime the application of an $n = 3$ field tends to maintain a large rotation (close to the neoclassical offset). When the rotation is forcibly reduced by changing the neutral beam torque, the confinement increases.

6. Test of QH-mode requirements

Because the theory of the EHO is based on single fluid MHD, it makes no distinction between the fluid toroidal rotation and ω_E, the species independent toroidal rotation driven by the radial electric field. These recent DIII-D experiments show that the shear in ω_E is the important rotational shear for QH-mode operation, rather than the shear in the measured rotation of the carbon impurity ions (commonly assumed as a proxy for the fluid rotation). The rotation profiles measured at low NBI torque show that a large shear in the edge velocity of carbon impurity ions is not required to sustain QH-mode with NRMFs. An example is shown in figure 9, which compares the rotation profiles measured at the QH-mode threshold observed in discharges with and without NRMF. These discharges have been discussed earlier, in relation to figure 2. Note that in this figure the linear velocity, not the angular velocity, is plotted. For both discharges, the edge shear is quite low in the profiles of the toroidal velocity of the carbon impurity ions, V_ϕ (e.g. compare with figure 4 in [7]). On the other hand, the edge shear is high and nearly equal in the profiles of the toroidal $E \times B$ velocity, V_E, particularly when evaluated over the outer half of the pedestal width. This narrow localization of the important part of the V_E profile is consistent with previous observations that the EHO is localized about 2 cm inside the separatrix near the top of the H-mode pedestal (see figure 6 in [33]) and that a large V_E shear is conserved at the very edge of the plasma in QH-modes observed under various conditions (see figures 10 and 14 in [33]). Figure 9 also shows the profiles of the measured poloidal velocity, V_θ, which is used in the derivation of V_E:

$$V_E = R\omega_E = R\frac{\partial P_C/\partial\psi}{6n_C e} + V_\phi - \frac{B_\phi V_\theta}{B_\theta}. \qquad (3)$$

The correlation between QH-mode edge and large shear in the edge ω_E rotation holds well in the cases analysed so far, when the shear is evaluated across the outer half of the H-mode pedestal (last 2% to 3% of the poloidal flux). Figure 10 shows a plot of the shear ($\Delta\Omega/\Delta r$) in carbon ion angular rotation speed $\Omega = V_\phi/R$ versus the shear in the ω_E rotation ($\Delta\omega_E/\Delta r$), for a database of 15 discharges with different edge characteristics. Each data point is a different discharge, except for the points connected by a line, which describe the time evolution of a single discharge. The database includes discharges with single null divertor and double null divertor cross-section shape; co- and counter-rotation; β_N in the range 1.4–3.3; and electron density in the range (2.3–9.0) $\times 10^{19}$ m^{-3} for ELMing discharges, and in the range (2.3–3.5) $\times 10^{19}$ m^{-3} for QH-mode discharges. The rotation shear is evaluated as a two point

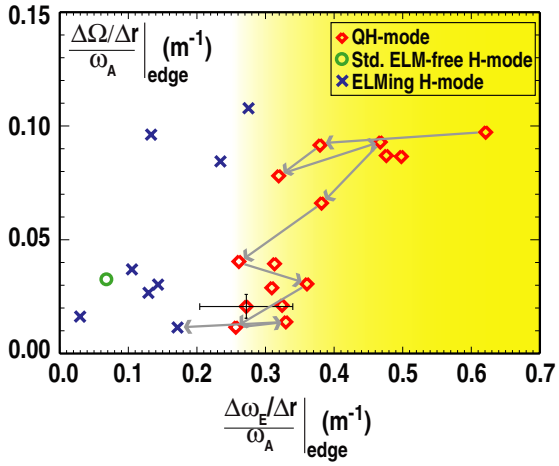

Figure 10. Edge shear in C VI impurity ion rotation versus edge shear in ω_E rotation for discharges with different H-mode edge characteristics. Shear is evaluated across the outer half of the H-mode pedestal width, and is normalized to the local Alfvén frequency. The grey line connects data for a single discharge (137234 of figure 2), evolving during the NBI torque ramp-down from a QH-mode phase to ELMing H-mode.

difference between the pedestal midpoint and the boundary. In order to compare discharges under different conditions, the rotation is normalized to the local Alfvén frequency, which is the relevant MHD frequency. A boundary near

$$\left.\frac{\Delta\omega_E/\Delta r}{\omega_{\rm A}}\right|_{\rm edge} \sim 0.25\,{\rm m}^{-1}$$

emerges between discharges that exhibit a QH-mode edge and discharges that are ELMing or standard ELM-free H-modes. These results suggest that the ω_E rotation is a better proxy for the fluid rotation near the plasma edge than the impurity ion rotation, and a more relevant rotation parameter for QH-mode access is the ω_E rotation shear at the very edge of the plasma, rather than the impurity ion edge rotation shear. However, these experiments do not discriminate against the rotation shear of the main ions, which was not measured.

7. Summary

In summary, recent DIII-D experiments have demonstrated new ways in which static non-axisymmetric magnetic fields can improve the tokamak configuration. The counter-$I_{\rm p}$ torque driven by $n = 3$ NRMFs can be used to replace the torque driven by NBI to maintain the edge rotation shear required for ELM-stable operation in QH-mode even with zero-net NBI torque. Furthermore, the application of the $n = 3$ NRMFs increases plasma resilience to locked modes and allows access to a region of parameter space that, with significant beta and zero-net NBI torque and near-zero core plasma rotation, is otherwise forbidden. Surprisingly, in this regime the energy confinement quality increases with lower counter-rotation.

The physics basis of this regime is strongly connected to theory. Comparisons of the observed NRMF torque to neoclassical theory predictions show good agreement. Observations of a threshold edge rotation shear for QH-mode operation, postulated by theory, persist even at very low plasma rotation, and indicate that the important shear is in the ω_E rotation. The surprising improvement in energy confinement observed at low rotation is consistent with the paradigm of $E \times B$ flow shear suppression of turbulence. The improved MHD stability in the presence of the NRMF supports the theory of NTM inhibition by an externally applied helical field.

By overcoming the long standing limitation of relying on strong NBI torque for QH-mode access, these research results have opened a path towards QH-mode utilization as an ELM-stable high confinement regime for the self-heated burning plasma scenario where the torque from neutral beam injection is expected to be small or absent. The strong theory-experiment coupling provides the necessary basis from which extrapolations to ITER and the reactor regime can be launched. In the near future, further theoretical work should try to improve the connection formulae between various collisionality regimes, and further experiments will be aimed at reproducing the results described in this paper in different tokamak devices, as well as at more ITER-relevant values of the edge safety factor ($q_{95} \sim 3$), and extending the zero NBI torque constraint to the entire plasma evolution.

Acknowledgment

This work was supported by the US Department of Energy under DE-FC02-04ER54698, DE-FG02-04ER54761, DE-AC02-09CH11466 and DE-FG02-08ER54984. The authors wish to thank T.H. Osborne for his support in the analysis of pedestal data, and E.J. Strait and T.L. Rhodes for helpful discussions.

Appendix. The ITER equivalent NBI torque in DIII-D

In this appendix we show the result of one possible criterion of equivalence between the NBI torque in ITER and DIII-D. In this criterion, the NBI torque in DIII-D, $T_{\rm NB,1}$, is equivalent to the NBI torque in ITER, $T_{\rm NB,2}$, when the NBI-driven rotations in the two tokamaks are the same:

$$\omega_{\rm NB,1} = \omega_{\rm NB,2}. \tag{A1}$$

Using a 0D model of torque balance:

$$T_{\rm NB} = \frac{L_{\rm NB}}{\tau_L}, \tag{A2}$$

the NBI-driven rotation is

$$\omega_{\rm NB} = \frac{L_{\rm NB}}{I} = \frac{T_{\rm NB}\tau_L}{I}, \tag{A3}$$

where L is the total toroidal NBI-driven angular momentum, I is the toroidal moment of inertia and τ_L is the angular momentum confinement time. Therefore, according to the equivalence definition in (A1), the DIII-D NBI torque equivalent to the ITER NBI torque is

$$T^{\rm e}_{\rm NB,1} = T_{\rm NB,2}\frac{I_1}{I_2}\frac{\tau_{L,2}}{\tau_{L,1}}. \tag{A4}$$

Assuming that the angular momentum confinement times scale like the energy confinement times, and using for DIII-D the parameter values of discharge 141439, and for ITER the values for the baseline scenario (Scenario 2) [34], the DIII-D NBI torque equivalent to the expected ITER NBI torque is obtained:

$$\frac{I_1}{I_2} = \frac{3.59 \times 10^{-6}}{1.07 \times 10^{-2}} = 3.36 \times 10^{-4}, \tag{A5}$$

$$\frac{\tau_{E,2}}{\tau_{E,1}} = \frac{3.7}{0.15} = 25, \tag{A6}$$

$$T_{\mathrm{NB},2} \approx 35\,\mathrm{Nm}, \tag{A7}$$

$$T^{\mathrm{e}}_{\mathrm{NB},1} \approx 0.01 T_{\mathrm{NB},2} \rightarrow 0.35\,\mathrm{Nm}. \tag{A8}$$

References

[1] Lang P.T. *et al* 2008 *Nucl. Fusion* **48** 095007
[2] Degeling A.W. *et al* 2003 *Plasma Phys. Control. Fusion* **45** 1637
[3] Evans T.E. *et al* 2006 *Nature Phys.* **2** 419
[4] Greenfield C.M. *et al* 2001 *Phys. Rev. Lett.* **86** 4544
[5] Burrell K.H. *et al* 2005 *Phys. Plasmas* **12** 056121
[6] Snyder P.B. *et al* 2007 *Nucl. Fusion* **47** 961
[7] Burrell K.H. *et al* 2009 *Phys. Rev. Lett.* **102** 155003
[8] Garofalo A.M. *et al* 2010 *Proc. 23rd Int. Conf. on Fusion Energy (Daejon, Korea, 2010)* (Vienna: IAEA) paper EXS/1-2 http://www-pub.iaea.org/mtcd/meetings/PDFplus/2010/cn180/cn180_papers/exs_1-2.pdf
[9] Cole A.J. *et al* 2007 *Phys. Rev. Lett.* **99** 065001
[10] Garofalo A.M. *et al* 2008 *Phys. Rev. Lett.* **101** 195005
[11] Aymar R., Barabaschi P. and Shimomura Y. 2002 *Plasma Phys. Control. Fusion* **44** 519
[12] Snyder P.B. *et al* 2009 *Nucl. Fusion* **49** 085035
[13] Jackson G.L. *et al* 2003 *Proc. 30th EPS Conf. on Controlled Fusion and Plasma Physics (St Petersburg, Russia, 2003)* vol 27A (ECA) p P-4.47. http://epsppd.epfl.ch/StPetersburg/PDF/P4_047.pdf
[14] Solomon W.M. *et al* 2010 *Phys. Plasmas* **17** 056108
[15] Rice J.E. *et al* 1998 *Nucl. Fusion* **38** 75
[16] Cole A.J., Callen J.D., Solomon W.M., Garofalo A.M., Hegna C.C., Lanctot M.J. and Reimerdes H. 2011 *Phys. Rev. Lett.* **106** 225002
[17] Park J.-K., Boozer A.H. and Glasser A.H. 2007 *Phys. Plasmas* **14** 052110
[18] Park J.-K., Boozer A.H. and Menard J.E. 2009 *Phys. Rev. Lett.* **102** 065002
[19] Shaing K.C. 2003 *Phys. Plasmas* **10** 1443
[20] Shaing K.C. *et al* 2008 *Phys. Plasmas* **15** 082506
[21] Shaing K.C., Sabbagh S.A. and Chu M.S. 2009 *Plasma Phys. Control. Fusion* **51** 035009
[22] Yushmanov P.N. *et al* 1990 *Nucl. Fusion* **30** 1999
[23] Liang Y. 2009 *36th EPS Conf. on Plasma Phys. (Sofia, Bulgaria, 2009)* vol 33E (ECA) O-5.062 http://epsppd.epfl.ch/Sofia/PDF/O5_062.pdf
[24] McKee G.R., Fonck R.J., Shafer M.W., Uzun-Kaymak I.U. and Yan Z. 2010 *Rev. Sci. Instrum.* **81** 10D741
[25] Schmitz L. *et al* 2008 *Rev. Sci. Instrum.* **79** 10F113
[26] Shaing K.C. and Crume Jr E.C. 1989 *Phys. Rev. Lett.* **63** 2369
[27] Biglari H., Diamond P.H. and Terry P.W. 1990 *Phys. Fluids* B **2** 1
[28] Hahm T.S. and Burrell K.H. 1995 *Phys. Plasmas* **2** 1648
[29] Staebler G.M., Kinsey J.E. and Waltz R.E. 2005 *Phys. Plasmas* **12** 102508
[30] Synakowski E.J. *et al* 1997 *Phys. Rev. Lett.* **78** 2972
[31] Yu Q. *et al* 2000 *Phys. Rev. Lett.* **85** 2949
[32] La Haye R.J. *et al* 2002 *Phys. Plasmas* **9** 2051
[33] Burrell K.H. *et al* 2004 *Plasma Phys. Control. Fusion* **46** A165–A178
[34] Budny R.V., Andre R., Bateman G., Halpern F., Kessel C.E., Kritz A. and McCune D. 2008 *Nucl. Fusion* **48** 075005